Transform-Limited X-Ray Pulse Generation from a High-Brightness Self-Amplified Spontaneous-Emission Free-Electron Laser

B. W. J. McNeil,[1,*] N. R. Thompson,[1,2,†] and D. J. Dunning[1,2,‡]
[1]University of Strathclyde (SUPA), Glasgow G4 0NG, United Kingdom
[2]ASTeC, Daresbury Laboratory, Warrington WA4 4AD, United Kingdom
(Received 23 December 2012; published 26 March 2013)

A method to achieve high-brightness self-amplified spontaneous emission (HB-SASE) in the free-electron laser (FEL) is described. The method uses repeated nonequal electron beam delays to delocalize the collective FEL interaction and break the radiation coherence length dependence on the FEL cooperation length. The method requires no external seeding or photon optics and so is applicable at any wavelength or repetition rate. It is demonstrated, using linear theory and numerical simulations, that the radiation coherence length can be increased by approximately 2 orders of magnitude over SASE with a corresponding increase in spectral brightness. Examples are shown of HB-SASE generating transform-limited FEL pulses in the soft x-ray and near transform-limited pulses in the hard x-ray. Such pulses may greatly benefit existing applications and may also open up new areas of scientific research.

DOI: 10.1103/PhysRevLett.110.134802 PACS numbers: 41.60.Cr

In the x-ray region of the spectrum self-amplified spontaneous emission (SASE) free-electron lasers (FELs) are currently opening up new frontiers across science [1–6]. Although SASE FELs have brightness up to 10^8 times greater than laboratory sources their full potential is limited by a relatively poor temporal coherence. In this Letter, a high-brightness SASE (HB-SASE) FEL is described which may significantly improve the temporal coherence towards the transform limit, enhancing the spectral brightness and potentially enabling x-ray FELs to enhance their existing scientific capability and to access new experimental regimes.

One of the applications that may benefit is resonant inelastic x-ray scattering (RIXS) [7] which requires substantial incident photon flux to collect sufficient spectra with a high enough resolution in energy and momentum in a reasonable time. RIXS has evolved greatly over the last decades, due to increases in photon flux from synchrotron sources then later x-ray FELs, as well as advances in instrumentation. Each increase in resolution has revealed new details in material excitation spectra. Further improvement may extend study to, e.g., single magnons in small exchange systems and the full dispersion curves of superconducting gaps. New applications made possible by Fourier-transform limited x-ray pulses may include time-resolved x-ray spectroscopy of chemical dynamics, or quantitative studies of molecular and cluster fragmentation, where high repetition rate pulses of controlled temporal profile are essential for systematic studies of nonlinear phenomena [8].

In the SASE FEL [9,10], a relativistic bunch of electrons with a Lorentz factor of $\gamma \gg 1$ enters an undulator comprising an array of transverse, alternating polarity dipole magnets of period λ_u. The undulator magnetic fields cause the electrons to oscillate transversely and emit initially incoherent radiation. A cooperative (or collective) instability in the coupled electron-radiation system may cause an exponential gain in the radiation field and an electron microbunching at the resonant radiation wavelength $\lambda_r = \lambda_u(1 + \bar{a}_u^2)/2\gamma^2$, where $\bar{a}_u$ is the rms undulator parameter, proportional to the undulator period and magnetic field. The interaction is a positive feedback process—the electron-radiation coupling drives the radiation phase giving a greater electron microbunching at the resonant wavelength and greater coherent radiation emission [6]. The process leaves the linear regime and saturates when the electrons become strongly bunched at the radiation wavelength and then begin to debunch. In the linear regime the power growth is given by $P(z) \sim (P_0/9) \times \exp(\sqrt{3}z/l_g)$ where the nominal gain length $l_g \equiv \lambda_u/4\pi\rho$ with ρ the dimensionless FEL parameter [9]. This type of collective process also describes several other particle-radiation interactions, such as the collective atomic recoil laser [11], collective Rayleigh scattering from linear dielectric particles [12] or collective scattering from the electron-hole plasma in semiconductors [13].

A significant difference between the FEL and these latter interactions is the relativistic speed of the electron bunch as it propagates through the FEL. In each undulator period λ_u a wave front at resonant radiation wavelength λ_r propagates through the electron beam a distance λ_r—this is referred to as ''slippage''. On propagating through one gain length of the undulator, a wave front propagates through the electron beam a distance $l_c \equiv \lambda_r/4\pi\rho \ll l_g$. This ''cooperation length'' l_c therefore defines the scale at which collective effects evolve throughout the electron beam, and so how the temporal coherence of the radiation field evolves from the initially spontaneous noise. For a sufficiently long electron beam, different regions along the beam develop from the localized noise source autonomously and are therefore uncorrelated in phase. In this

sense, the SASE process can be considered as a "localized" collective process. At saturation the SASE output then comprises a series of phase-uncorrelated "spikes" which can be shown to be separated by $\lesssim 2\pi l_c$ [14]. Typically, in the x-ray the electron bunch length $l_b \gg 2\pi l_c$, so the output comprises many such spikes and the pulse is far from Fourier-transform limited and consequently of reduced spectral brightness from that potentially available.

Several methods may be used to improve the temporal coherence of the SASE FEL output. These can be divided into two general classes. In the first class, an externally injected source of good temporal coherence "seeds" the FEL interaction so that noise effects are reduced. This seed field may be either at the resonant radiation wavelength, where available, or at a subharmonic wavelength which is then up-converted within the FEL. These methods, which include high gain harmonic generation [15–18] and echo-enabled harmonic generation [19,20], rely on a synchronized external seed at the appropriate wavelength, pulse energy, and repetition rate. In the second class, the coherence is created by optical manipulation of the FEL radiation itself, for example by spectrally filtering the SASE emission at an early stage for subsequent reamplification to saturation in a self-seeding method [21–24], or via the use of an optical cavity [25–32]. Methods in this class rely on potentially complex material-dependent optical systems which limit the ease and range of wavelength tuning. If an optical cavity is used, the electron source repetition rate should also be in the MHz regime to enable a practical cavity length.

The HB-SASE method described in this Letter requires no external seeding or photon optics and is applicable at any wavelength and repetition rate. It works by using a series of magnetic chicanes inserted between each section of a long sectional undulator. The chicanes periodically delay the electron bunch with respect to the copropagating radiation field. The delays have two main effects. First, a radiation wave front propagates at a rate through the electron beam which can be significantly greater than in SASE—the slippage rate is increased. Second, if the undulator sections are shorter than the gain length l_g, and the chicanes introduce delays which are greater than the cooperation length l_c, then the localized nature of the collective interaction may be broken, so inhibiting the formation of the phase-uncorrelated radiation spikes associated with SASE. The electron-radiation interaction distance over which temporal coherence can be developed therefore becomes much greater than the $\lesssim 2\pi l_c$ of SASE [14], and potentially towards the total length that a resonant wave front propagates through the electron beam to saturation. This process is aided by the relatively fast rate of change of the radiation phase which can occur in the linear regime [6] and which allows the temporal coherence to propagate via a radiation phase which evolves with much greater uniformity than can occur in SASE.

An initial study over a limited parameter range [33], and contemporaneous work [34,35], have demonstrated the basic principle of improving the temporal coherence. It is now shown in this Letter that by delocalizing the collective interaction as described above, the coherence length of the radiation may in fact be extended by orders of magnitude with a corresponding enhancement in the spectral brightness. Hence the name high-brightness SASE (HB-SASE).

The potential of HB-SASE is demonstrated using a FEL numerical simulation code that solves the universally scaled one-dimensional FEL equations [36]

$$\frac{d\theta_j}{d\bar{z}} = p_j \tag{1}$$

$$\frac{dp_j}{d\bar{z}} = -[A(\bar{z},\bar{z}_1)\exp(i\theta_j) + \text{c.c.}] \tag{2}$$

$$\left(\frac{\partial}{\partial\bar{z}} + \frac{\partial}{\partial\bar{z}_1}\right)A(\bar{z},\bar{z}_1) = \chi(\bar{z}_1)b(\bar{z},\bar{z}_1). \tag{3}$$

In this scaling, the independent parameters are the combined interaction distance through the undulator which is scaled by the gain length, $\bar{z} = z/l_g$, and the distance in the electron beam rest frame which is scaled by the cooperation length, $\bar{z}_1 = (z - c\bar{\beta}_z t)/l_c$. The dependent electron-radiation parameters are defined as follows: $\theta_j = (k + k_u)z - \omega t_j$ is the ponderomotive phase of the jth electron; $p_j = (\gamma_j - \gamma_r)/\rho\gamma_r$ is its scaled energy; $b(\bar{z},\bar{z}_1) \equiv \langle e^{-i\theta(\bar{z})}\rangle|_{\bar{z}_1}$ is the electron bunching factor for which $0 \le |b| < 1$ and is the average over the electrons contained within the ponderomotive well centered at $\bar{z}_1$ at distance through the interaction region $\bar{z}$; $\chi(\bar{z}_1) = I(\bar{z}=0,\bar{z}_1)/I_{\text{pk}}$ is the current weight factor where $I(\bar{z}=0,\bar{z}_1)$ describes the electron pulse current distribution of peak value I_{pk} at the entrance to the FEL interaction region; $A(\bar{z},\bar{z}_1)$ is the scaled complex radiation field envelope of magnitude approximated by $|A|^2 \sim P_{\text{rad}}/\rho P_{\text{beam}}$ with P_{rad} and P_{beam} the radiation and peak electron beam powers, respectively. The scaled frequency is $\bar{\omega} = (\omega - \omega_r)/2\rho\omega_r$.

The effect of a chicane is to delay the electrons by a longitudinal shift of $\bar{\delta}$, so that $\bar{z}_1 \to \bar{z}_1 - \bar{\delta}$. Radiation wave front propagation in $\bar{z}_1$ within each undulator section is a constant $\bar{l}$, so the total relative displacement for the nth undulator-chicane module is $\bar{s}_n = \bar{l} + \bar{\delta}_n$. For equal delays ($\bar{\delta}_n = \bar{\delta}$, a constant) the system is identical to that of the mode-coupled FEL [37], where the frequency spectrum displays discrete sideband modes at spacing $\Delta\bar{\omega} = 2\pi/\bar{s}$ and the field in the temporal domain is strongly modulated with period $\bar{s} = \bar{l} + \bar{\delta}$. In HB-SASE, however, the chicane delays of the nth undulator-chicane module $\bar{\delta}_n$, are not equal. With an appropriately chosen sequence of unequal delays, the set of sideband mode frequencies supported by each undulator-chicane module can be made unique. Only those frequencies immediately about the resonant

frequency $\bar{\omega} = 0$ will then receive amplification—the process may thus be considered as a sequential filtering of unwanted frequencies, or a self-seeding of the growing radiation field.

The FEL equations (1)–(3) can be linearized using collective variables [38], and solved in the frequency domain via a Fourier-Laplace transformation. A linear solution of the interaction to the end of the nth undulator-chicane module is obtained by sequentially applying the solution using the output of module (n-1) as the initial conditions for the nth module to give:

$$\tilde{x}_j^{(n)} = -e^{i\bar{\omega}\bar{\delta}_j^{(n-1)}} \sum_{k=1}^{3} \tilde{x}_k^{(n-1)} \sum_{p=1}^{3} \frac{a_{jk}(\lambda_p) e^{i\lambda_p \bar{l}}}{\prod_{q\neq p} (\lambda_p - \lambda_q)} \qquad (4)$$

with $j = 1, \ldots, 3$ for the column vector of linear variables:

$$\tilde{x}^{(n)} = \begin{bmatrix} \tilde{b}^{(n)} \\ \tilde{P}^{(n)} \\ \tilde{A}^{(n)} \end{bmatrix} \quad \text{and}$$

$$a_{jk} = \begin{bmatrix} -\lambda(\lambda+\bar{\omega}) & (\lambda+\bar{\omega}) & i \\ 1 & -\lambda(\lambda+\bar{\omega}) & -i\lambda \\ i\lambda & -i & -\lambda^2 \end{bmatrix}, \qquad (5)$$

where $\lambda_{p,q}$ are roots of the characteristic equation $\lambda^3 + \bar{\omega}\lambda^2 + 1 = 0$ and a variable dependence on $\bar{\omega}$ is assumed. After the nth undulator section a chicane delay of $\bar{\delta}^{(n)}$ in $\bar{z}_1$ of the electron variables $\tilde{x}_1^{(n)} \equiv \tilde{b}^{(n)}$ and $\tilde{x}_2^{(n)} \equiv \tilde{P}^{(n)}$ is achieved using the Fourier shift theorem by multiplying by $\exp(i\bar{\omega}\bar{\delta}_j^{(n)})$, where $\bar{\delta}_{1,2}^{(n)} = \bar{\delta}^{(n)}$. The field variable $\tilde{x}_3^{(n)} \equiv \tilde{A}^{(n)}$ is unaffected by the chicane, so that $\bar{\delta}_3^{(n)} = 0$.

The total gain bandwidth envelope of (4) is the single undulator section spectrum, as for the mode coupled case of Ref. [37]; i.e., it is a sinc function with the first zero at $\bar{\omega} = 2\pi/\bar{l}$. The linear solution can now be used to optimize a sequence of chicane delays. For example, the sequence used in the results presented in this Letter is given by $\bar{s}_n = \mathbb{P}_n \bar{s}_1/2$ where $\bar{s}_1 = \bar{l} + \bar{\delta}_1$ and $\mathbb{P}_n$ are a series of primes with $\mathbb{P}_1 = 2$. It is found that, for this sequence, in order for no common modes to exist within the gain bandwidth $\bar{s}_1 \leq 2\bar{l}$ must be satisfied, and similarly for no common modes within the FWHM bandwidth $\Delta\bar{\omega}_{\mathrm{FWHM}} \simeq 5.4/\bar{l}$ [37], it is necessary for $\bar{s}_1 < 4.65\bar{l}$. With some empirical adjustment it may be possible to optimize further this particular delay sequence and circumvent these limits. Other sequences of delays (for example, random variation about a set mean or quasiperiodic [39]) have also been shown in simulations to be effective, and can be optimized using the linear solution (4).

For $\bar{l} = 0.5$ and any sequence of chicane delays, the FWHM bandwidth as measured from (4) around the resonant frequency $\bar{\omega} = 0$ is given by $\Delta\bar{\omega} \simeq 4\pi/\bar{S}$, where $\bar{S} \equiv \sum_n \bar{s}_n$ is the total slippage.

A typical HB-SASE simulation is now shown which demonstrates a large increase in radiation coherence length over normal SASE. A constant current [$\chi(\bar{z}_1) = 1$], cold (no energy spread), long electron beam of scaled length $\bar{l}_e = 4000$ was used. Undulator sections of scaled length $\bar{l} = 0.5$ and a sequence of chicane delays with $\bar{s}_1 = 4\bar{l}$ were used as described above. Effects arising from emission at the rear of the electron pulse have been omitted. Figure 1 plots the average scaled pulse optical power $\langle|A|^2\rangle$, and the scaled radiation coherence length $\bar{l}_{\mathrm{coh}} = \int |g(\bar{\tau}_1)|^2 d\bar{\tau}_1$ as a function of $\bar{z}$, where $g(\bar{\tau}_1) = \langle A^*(\bar{z}_1)A(\bar{z}_1 + \bar{\tau}_1)\rangle / \langle A^*(\bar{z}_1)A(\bar{z}_1)\rangle$ [40]. The integral in $\bar{\tau}_1$ is taken over the total accumulated slippage $\bar{S}$ for both the SASE and HB-SASE simulations. The SASE saturation length is $\bar{L}_{\mathrm{sat}} \approx 12.0$, with a coherence length in units of $\bar{z}_1$ of $\bar{l}_{\mathrm{coh}} \approx 3.4$ and rms bandwidth $\sigma_{\bar{\omega}} = 0.5$. This is in good agreement with SASE behavior close to saturation [14,41,42] and in particular with the relation, written in scaled form here, of $\sigma_{\bar{\omega}}\bar{l}_{\mathrm{coh}} \approx \sqrt{\pi}$. For HB-SASE the saturation length is slightly increased to $\bar{L}_{\mathrm{sat}} \approx 14.5$ with a mean saturated power similar to SASE. However, the coherence length of HB-SASE has increased by 2 orders of magnitude to $\bar{l}_{\mathrm{coh}} = 393$ with a bandwidth reduced to $\sigma_{\bar{\omega}} = 0.0045$, to give a corresponding increase in spectral brightness of over 2 orders of magnitude over SASE. Note that the SASE relation of $\sigma_{\bar{\omega}}\bar{l}_{\mathrm{coh}} \approx \sqrt{\pi}$ remains valid in the HB-SASE simulation. A preliminary study of HB-SASE shot-to-shot pulse energy fluctuations also demonstrates a SASE-like gamma function dependence [41]. It is seen that the SASE coherence length $\bar{l}_{\mathrm{coh}}$, evolves little after the first three gain lengths, reaching half its saturation value by $\bar{z} = 3$ and thereafter growing more slowly than the accumulated slippage $\bar{S}$. This behavior is again in good agreement with that predicted in Ref. [41], and is consistent with the localized growth of the radiation spikes uncorrelated in phase. Conversely, for HB-SASE, $\bar{l}_{\mathrm{coh}}$ evolves little for the first three gain lengths, then grows exponentially with a growth rate greater than $\bar{S}$. This appears consistent with a more delocalized interaction as

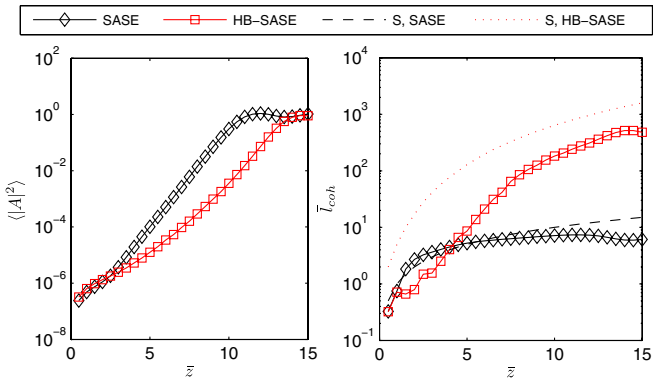

FIG. 1 (color online). Evolution with propagation distance $\bar{z}$ of the scaled optical power $\langle|A|^2\rangle$, and radiation coherence length $\bar{l}_{\mathrm{coh}}$. Also shown is the accumulated total slippage $\bar{S}(\bar{z})$.

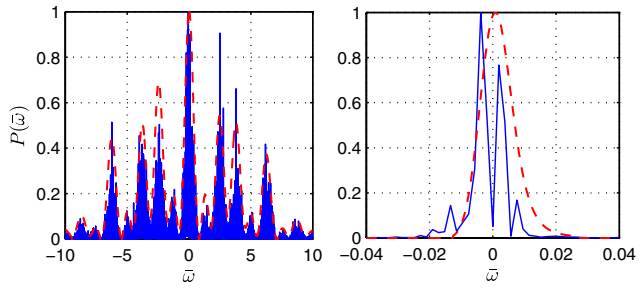

FIG. 2 (color online). Comparison of the radiation spectra from the simulation results (blue, solid line) and by the linear theory (4) (red, dashed line), at $\bar{z} = 1.5$ (left) and $\bar{z} = 12.5$ (right). Plots are scaled with respect to their peak values.

discussed above, where initially the coherence takes longer to develop, but then evolves to become slowly varying over a range approaching the accumulated slippage $\bar{S}$ (not shown).

Agreement between the radiation spectra from the simulation results and that predicted by the linear theory of (4), is shown in Fig. 2 near the beginning of the interaction and approaching saturation where the FWHM bandwidth is measured as $\Delta\bar{\omega} \approx 0.011$.

A practical example is now shown of HB-SASE applied to a hard x-ray FEL. The parameters are $\lambda_r = 0.13$ nm, beam energy $E = 14.7$ GeV, peak current $I_{\rm pk} = 3000$ A, bunch charge $Q = 10$ pC, $\lambda_u = 30$ mm, and $\rho = 4.17 \times 10^{-4}$. The delays are set so that at saturation the total slippage is the FWHM electron bunch length, giving $\bar{s}_1 = 1.08\bar{l}$. The undulator modules have length $\bar{l} = 0.5$ equivalent to $L_u = 2.85$ m. The results are shown in S.I. units. Figure 3 shows the pulse profiles and spectra of SASE and HB-SASE at saturation. The efficacy of HB-SASE is clearly demonstrated—the SASE pulse is a chaotic sequence of phase uncorrelated spikes whereas the HB-SASE pulse is a near-single spike with slowly varying phase (not shown). For SASE, the coherence time $t_{\rm coh} = l_{\rm coh}/c = 0.27$ fs, in excellent agreement with Ref. [42], and $\sigma_\lambda/\lambda = 4.3 \times 10^{-4} \simeq \rho$, so that $\sigma_\omega t_{\rm coh} = 1.68 \approx \sqrt{\pi}$. For HB-SASE, $t_{\rm coh} = 7.0$ fs and $\sigma_\lambda/\lambda = 2.0 \times 10^{-5}$, so that $\sigma_\omega t_{\rm coh} = 2.03$, similar to the SASE scaling. The FWHM pulse durations and bandwidths at saturation give time-bandwidth products $\Delta\nu\Delta t = (1/\lambda)(\Delta\lambda/\lambda)c\Delta t = 32$ for SASE and $\Delta\nu\Delta t = 0.85$ for HB-SASE, indicating the HB-SASE output pulse is close to transform limited.

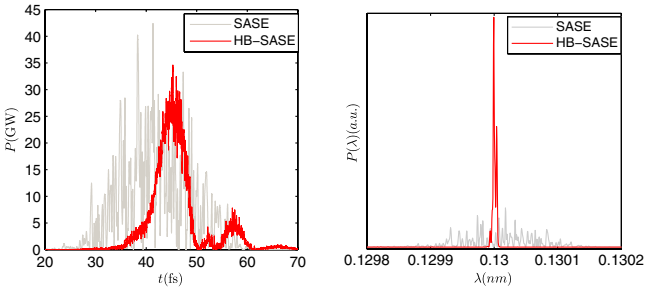

FIG. 3 (color online). Hard x-ray example at $\lambda_r = 0.13$ nm: the pulse profiles and spectra of SASE and HB-SASE.

Finally, a brief example is shown of a soft x-ray FEL operating at $\lambda_r = 1.24$ nm with $E = 2.25$ GeV, $I_{\rm pk} = 1200$ A and $Q = 200$ pC. Figure 4 shows the results at saturation. For HB-SASE, $\Delta\nu\Delta t = 0.53$, indicating the output pulse is again close to transform limited.

In this Letter, a HB-SASE coherence length of 2 orders of magnitude greater than the equivalent SASE was obtained using undulator section lengths of $\bar{l} = 0.5$. Increasing $\bar{l}$ further to 1.0 and 2.0, the maximum coherence lengths are reduced to factors of approximately 50 and 10 times that of SASE, respectively. As most current FELs have been designed so that module lengths $\bar{l} \gtrsim 1$, this suggests that HB-SASE may be successfully applied, but not optimally, at existing facilities by inclusion of suitably compact chicanes between undulator sections.

The isochronous delay chicanes used here [43] do not affect the rate of electron microbunching. Simulation studies show that a deviation from nonisochronicity by $<10\%$ of the longitudinal dispersion of a standard four-dipole chicane does not detrimentally affect the results. The reoptimized chicane design of Ref. [43] meets this criteria for the parameters of the hard x-ray HB-SASE FEL. The electron beam energy spread should satisfy $\sigma_\gamma/\gamma_r \lesssim 10^{-4}$ to prevent electron debunching. The isochronous chicane design also limits the dependence of electron delay on transverse position and angle, so that for normalized emittance of $\epsilon_n \approx 1$ mm mrad, a common value in the x-ray FEL regime, there is negligible longitudinal shear for a matched beam. A study of the efficacy of standard non-isochronous 4-dipole chicanes for HB-SASE has shown that the improvement in longitudinal coherence over SASE is limited to a factor of approximately ten for an ideal cold beam. Inclusion of energy chirp and spread would be expected to limit this further. An alleviation option may be to introduce occasional "correction" chicanes with a strong negative compaction [44].

The high-brightness SASE FEL may enable the generation of transform-limited x-ray pulses. By delocalizing the collective FEL interaction, the radiation coherence length dependence on the FEL cooperation length is broken.

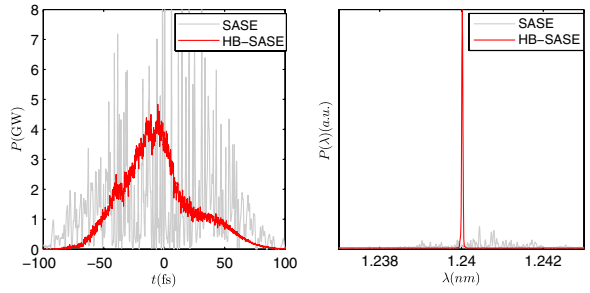

FIG. 4 (color online). Soft x-ray example at $\lambda_r = 1.24$ nm.

While the technique described here was applied to a high-gain FEL, the similarity of the FEL process to other collective systems may open a route to new methods for coherence control and noise reduction in such systems.

The authors would like to thank James Jones for helpful discussions. This work received support from STFC Memorandum of Agreement No. 4163192.

*b.w.j.mcneil@strath.ac.uk
†neil.thompson@stfc.ac.uk
‡david.dunning@stfc.ac.uk

[1] W. Ackermann *et al.*, Nat. Photonics **1**, 336 (2007).
[2] P. Emma *et al.*, Nat. Photonics **4**, 641 (2010).
[3] H. Tanaka *et al.*, SCSS X-FEL Conceptual Design Report, RIKEN Harima Institute, 2005.
[4] H. Tanaka *et al.*, Nat. Photonics **6**, 540 (2012).
[5] C. J. Bocchetta *et al.*, FERMI@Elettra Conceptual Design Report No. ST/F-TN-07/12 (Sincrotrone Trieste), 2007.
[6] B. W. J. McNeil and N. R. Thompson, Nat. Photonics **4**, 814 (2010).
[7] L. J. P. Ament, M. van Veenendaal, T. P. Devereaux, J. P. Hill, and J. van den Brink, Rev. Mod. Phys. **83**, 705 (2011).
[8] J. Marangos *et al.*, New Light Source Conceptual Design Report, 2010.
[9] R. Bonifacio, C. Pellegrini, and L. Narducci, Opt. Commun. **50**, 373 (1984).
[10] A. M. Kondratenko and E. L. Saldin, Part. Accel. **10**, 207 (1980).
[11] R. Bonifacio and L. De Salvo, Nucl. Instrum. Methods Phys. Res., Sect. A **341**, 360 (1994).
[12] G. R. M. Robb and B. W. J. McNeil, Phys. Rev. Lett. **90**, 123903 (2003).
[13] G. R. M. Robb, B. W. J. McNeil, I. Galbraith, and D. A. Jaroszynski, Phys. Rev. B **63**, 165208 (2001).
[14] R. Bonifacio, L. De Salvo, P. Pierini, N. Piovella, and C. Pellegrini, Phys. Rev. Lett. **73**, 70 (1994).
[15] R. Bonifacio, L. De Salvo Souza, P. Pierini, and E. T. Scharlemann, Nucl. Instrum. Methods Phys. Res., Sect. A **296**, 787 (1990).
[16] I. Ben-Zvi, L. F. Di Mauro, S. Krinsky, M. G. White, and L. H. Yu, Nucl. Instrum. Methods Phys. Res., Sect. A **304**, 181 (1991).
[17] L. H. Yu, Phys. Rev. A **44**, 5178 (1991).
[18] L. H. Yu *et al.*, Science **289**, 932 (2000).
[19] G. Stupakov, Phys. Rev. Lett. **102**, 074801 (2009).
[20] D. Xiang *et al.*, Phys. Rev. Lett. **105**, 114801 (2010).
[21] J. Feldhaus, E. L. Saldin, J. R. Schneider, E. A. Schneidmiller, and M. V. Yurkov, Opt. Commun. **140**, 341 (1997).
[22] E. L. Saldin, E. A. Schneidmiller, Yu. V. Shvyd'ko, and M. V. Yurkov, Nucl. Instrum. Methods Phys. Res., Sect. A **475**, 357 (2001).
[23] G. Geloni, V. Kocharyan, and E. Saldin, J. Mod. Opt. **58**, 1391 (2011).
[24] J. Amann *et al.*, Nat. Photonics **6**, 693 (2012).
[25] R. Colella and A. Luccio, Opt. Commun. **50**, 41 (1984).
[26] K.-J. Kim, Y. Shvyd'ko, and S. Reiche, Phys. Rev. Lett. **100**, 244802 (2008).
[27] B. W. J. McNeil, IEEE J. Quantum Electron. **26**, 1124 (1990).
[28] D. C. Nguyen, R. L. Sheffield, C. M. Fortgang, J. C. Goldstein, J. M. Kinross-Wright, and N. A. Ebrahim, Nucl. Instrum. Methods Phys. Res., Sect. A **429**, 125 (1999).
[29] B. Faatz, J. Feldhaus, J. Krzywinski, E. L. Saldin, E. A. Schneidmiller, and M. V. Yurkov, Nucl. Instrum. Methods Phys. Res., Sect. A **429**, 424 (1999).
[30] Z. Huang and R. D. Ruth, Phys. Rev. Lett. **96**, 144801 (2006).
[31] B. W. J. McNeil, N. R. Thompson, D. J. Dunning, J. G. Karssenberg, P. J. M. van der Slot, and K.-J. Boller, New J. Phys. **9**, 239 (2007).
[32] D. J. Dunning, B. W. J. McNeil, and N. R. Thompson, Nucl. Instrum. Methods Phys. Res., Sect. A **593**, 116 (2008).
[33] N. R. Thompson *et al.*, Proc. IPAC, TUPE050 (2010) 2257.
[34] J. Wu and C. Pellegrini (private communication). Following submission of this Letter, the authors have received details of as yet unpublished, similar, works on both theoretical and experimental research in this field. The theoretical work, presented at the 34th International Free-Electron Laser Conference in Nara, Japan (2012), uses a series of geometrically increasing chicane delays to the electron beam. The experimental work, conducted at LCLS, introduces electron beam delays by using detuned undulator sections similar to that as described in Ref. [35].
[35] Dao Xiang, Yuantao Ding, Zhirong Huang, and Haixiao Deng, Phys. Rev. ST Accel. Beams **16**, 010703 (2013).
[36] R. Bonifacio, B. W. J. McNeil, and P. Pierini, Phys. Rev. A **40**, 4467 (1989).
[37] N. R. Thompson and B. W. J. McNeil, Phys. Rev. Lett. **100**, 203901 (2008).
[38] R. Bonifacio, C. Maroli, and N. Piovella, Opt. Commun. **68**, 369 (1988).
[39] J. A. Clarke, *The Science and Technology of Undulators and Wigglers* (Oxford University Press, New York, 2004).
[40] J. W. Goodman, *Statistical Optics* (John Wiley & Sons Inc., New York, 2000), Chap. 5.
[41] E. L. Saldin, E. A. Schneidmiller, and M. V. Yurkov, Opt. Commun. **148**, 383 (1998).
[42] E. L. Saldin, E. A. Schneidmiller, and M. V. Yurkov, New J. Phys. **12**, 035010 (2010).
[43] J. K. Jones *et al.*, Proc. IPAC, TUPPP069 (2012) 1759.
[44] H. L. Owen and P. H. Williams, Nucl. Instrum. Methods Phys. Res., Sect. A **662**, 12 (2012).